colloids and interfaces

MDPI

Article

The Precipitation of Calcium Carbonate in the Presence of Macromolecules Isolated from Corals

Jasminka Kontrec [1], Nives Matijaković Mlinarić [1], Damir Kralj [1], Giuseppe Falini [2], Atiđa Selmani [3], Stefano Goffredo [4] and Branka Njegić Džakula [1,*]

[1] Laboratory for Precipitation Processes, Division of Materials Chemistry, Ruđer Bošković Institute, Bijenička c. 54, 10000 Zagreb, Croatia; jasminka.kontrec@irb.hr (J.K.); nmatijak@irb.hr (N.M.M.); kralj@irb.hr (D.K.)
[2] Dipartimento di Chimica "Giacomo Ciamician", Alma Mater Studiorum-Universitá di Bologna, Via Selmi 2, 40126 Bologna, Italy; giuseppe.falini@unibo.it
[3] Pharmaceutical Technology and Biopharmacy, Institute of Pharmaceutical Sciences, University of Graz, Universitatsplatz 1, 8010 Graz, Austria; atida.selmani@uni-graz.at
[4] Department of Biological, Geological and Environmental Sciences, University of Bologna, Via Selmi 3, 40126 Bologna, Italy; s.goffredo@unibo.it
* Correspondence: bnjeg@irb.hr

Abstract

This study investigated the $CaCO_3$ spontaneous precipitation in the presence of soluble organic macromolecules (SOMs) extracted from the skeleton of Mediterranean colonial coral species, symbiotic *Cladocora caespitosa* (SOM-CCA) and asymbiotic *Astroides calycularis* (SOM-ACL). This approach was used as a model to explore biomineralization processes in marine organisms. The research was conducted in systems without or with the addition of Mg^{2+} (Mg/Ca molar ratio was 5:1) and/or SOMs (concentration range was 0.5–4 ppm). In the model system (system without Mg^{2+} or SOMs), only vaterite spherulites precipitated, while in the system with added Mg^{2+}, only aragonite irregular aggregates were observed. Although the addition of SOMs did not influence the polymorphic composition of the $CaCO_3$ precipitates, it led to noticeable changes in induction time and morphology of $CaCO_3$ crystals, and these effects were stronger in the presence of SOM-ACL. By comparing systems containing both Mg^{2+} and SOM with the model system as well as with systems where Mg^{2+} or SOMs were added individually, the dominant role of Mg^{2+} in the aragonite formation was observed. However, the combined effect of Mg^{2+} and both SOMs enhanced the inhibition of $CaCO_3$ precipitation. This inhibitory effect was particularly enhanced in the system combining Mg^{2+} and SOM-ACL.

Keywords: calcium carbonate; precipitation; corals; macromolecules; inhibition; magnesium

Academic Editor: Reinhard Miller

Received: 20 June 2025
Revised: 31 July 2025
Accepted: 13 August 2025
Published: 15 August 2025

Citation: Kontrec, J.; Matijaković Mlinarić, N.; Kralj, D.; Falini, G.; Selmani, A.; Goffredo, S.; Njegić Džakula, B. The Precipitation of Calcium Carbonate in the Presence of Macromolecules Isolated from Corals. *Colloids Interfaces* **2025**, *9*, 50. https://doi.org/10.3390/colloids9040050

1. Introduction

Calcium carbonate ($CaCO_3$) is one of the most abundant minerals on Earth and serves as an important model system in studies of biomineralization, crystallization, colloidal stability, and interfacial phenomena [1]. The precipitation of $CaCO_3$ from aqueous solutions is a complex physicochemical process involving a series of interdependent steps, including nucleation, crystal growth, and aggregation, all of which are highly sensitive to solution chemistry and interfacial interactions [2]. These phenomena are not only relevant in geochemical and biological settings, but also in a wide range of applied fields, including water treatment, materials science, and pharmaceuticals. At the core of $CaCO_3$ precipitation

behavior lies the interplay between surface energy, ion activity (with special emphasis on supersaturation as the main driving force for precipitation), and the presence of dissolved macromolecules [3–7]. Besides the mentioned three main factors, temperature [8], pH [9,10], ionic strength [11], hydrodynamics [10,12], and the presence of other additives [13–15] can also influence the precipitation of $CaCO_3$.

$CaCO_3$ can precipitate in several distinct solid phases, including three anhydrous crystalline polymorphs (calcite, aragonite, and vaterite) and three hydrated forms: amorphous calcium carbonate (ACC), calcium carbonate monohydrate (also called monohydrocalcite, MHC), and calcium carbonate hexahydrate. Among these, calcite is the most thermodynamically stable phase under standard conditions. In biological systems, $CaCO_3$ typically occurs in the form of calcite or aragonite due to the relative instability of the other modifications [1,16]. Nevertheless, even unstable phases such as ACC can occasionally be found as a transient precursor phase during mineralization processes [17–23]. Vaterite, although the least stable of the anhydrous polymorphs, also occurs in nature, often in association with biogenic activity [1]. Its presence has been reported in pathological calcifications such as pancreatic stones and heart valve deposits [24] as well as in certain biomineralized structures, including fish otoliths [25], crustacean statoliths [26], ascidian skeleton [27], and freshwater pearls [28]. Despite being the least common of the $CaCO_3$ polymorphs, vaterite serves as a useful model system; investigations of its nucleation, growth, and stabilization contribute to a deeper understanding of both biomineralization mechanisms and fundamental crystallization processes [12,29–31].

$CaCO_3$ represents a fundamental inorganic constituent of skeletal and structural elements in a wide range of marine calcifying organisms, such as mollusks, corals, algae, sponges, and foraminifera [1]. In these organisms, $CaCO_3$ precipitation takes place via biomineralization, a highly regulated process in which precipitation processes serve as the underlying mechanism for mineral phase formation. As mentioned earlier, among marine calcifiers, calcium carbonate most commonly occurs as either calcite or aragonite, with aragonite prevailing in organisms such as corals and mollusks. The dominance of aragonite in present-day oceans is closely linked to elevated magnesium ion (Mg^{2+}) concentrations, as the typical Mg/Ca molar ratio in seawater is approximately 5.2 [32]. Mg^{2+} significantly inhibits the growth of calcite crystals while enhancing aragonite formation, thus favoring aragonite as the precipitated phase in high-Mg environments [13,14,33]. Inhibition of calcite growth becomes increasingly pronounced when the Mg/Ca ratio exceeds 1–2 [34]. Furthermore, experimental data obtained under laboratory conditions show that at Mg/Ca ratios ≥ 4, similar to seawater, aragonite becomes the kinetically preferred $CaCO_3$ polymorph over magnesium-rich calcite [35,36]. In addition to promoting aragonite formation, Mg^{2+} can influence the stabilization and transformation of MHC and ACC. MHC typically forms in environments characterized by high concentrations of Mg^{2+} (high Mg/Ca molar ratios) [37,38]. It is generally believed to precipitate through a Mg-enriched amorphous calcium carbonate (ACC) precursor, which subsequently transforms into the crystalline MHC phase. Vereshchagin et al. [39] demonstrated that monohydrocalcite can incorporate significant amounts of Mg^{2+} and remain stable over long periods under dry conditions, challenging its traditional view as a short-lived intermediate phase. Also, Mg^{2+} is known to stabilize amorphous calcium carbonate (ACC) by inhibiting its transformation to crystalline phases [40–42]. This effect is primarily attributed to the high hydration enthalpy of Mg^{2+}, which limits the mobility and rearrangement of ions within the ACC matrix. In addition, Mg^{2+} may be incorporated into the porous structure of ACC or adsorbed at particle surfaces, further retarding dehydration and structural ordering. As a result, Mg^{2+} reduces the rate of crystallization and dissolution of ACC, thereby extending its lifetime in solution. Mg^{2+} ions exert both thermodynamic and kinetic control: they alter the solubility product of calcium

carbonate phases, interact with carbonate and hydrated calcium ion complexes in solution, and adsorb on growing crystal faces, thus modulating surface free energy and nucleation barriers. The selective adsorption of Mg^{2+} at specific lattice planes contributes to phase stabilization and polymorph control, key aspects of interface-mediated crystallization [13].

Biominerals that constitute the rigid structural elements of marine calcifying organisms are composed predominantly of calcium carbonate, yet they also incorporate a minor fraction of organic macromolecules known as the organic matrix. The significance of this organic component in biomineralization has long been recognized. These organic macromolecules are secreted by the organism and become embedded within the mineralized tissue, exerting functional control over the mineralization process. Although the organic matrix typically comprises only a small percentage of the total mass, it plays a pivotal role in directing polymorph selection and influencing crystal morphology [1]. The organic matrix is structurally and chemically diverse, comprising both insoluble and soluble components. Insoluble macromolecular frameworks, such as hydrophobic proteins and polysaccharides [1,43], primarily affect the spatial organization and aggregation of forming crystals [44–47]. In contrast, the soluble fraction, mainly composed of acidic proteins enriched in aspartic and glutamic acid residues [48], has been implicated in regulating nucleation, phase selection, and crystal growth behavior [49–52]. In addition to biogenic matrices, numerous synthetic organic molecules, such as low molecular weight compounds [53–56], polyelectrolytes [57,58], poly(amino acids) [59–61], and block copolymers [62–64], have been used as additives in studies aimed at modulating $CaCO_3$ crystallization pathways and stabilizing amorphous precursors. Despite these advances, many aspects of matrix–mineral interactions remain unresolved.

Although much of the current research has examined the effects of isolated organic or inorganic additives on calcium carbonate formation, it is important to acknowledge that biomineralization within living systems typically occurs in the presence of a multitude of interacting molecular species. Only a limited number of biomimetic studies have systematically investigated how multiple additives might jointly affect crystallization outcomes [65–67]. Some recent studies have explored combinations of amino acids and dye molecules, demonstrating that amino acids can significantly enhance the incorporation of dyes into growing crystals, far beyond what is achieved with dyes alone [68]. These findings highlight a promising strategy for designing advanced functional materials through additive combinations. In the context of biomineralization, such combined interactions are highly relevant, as the native mineralizing environment inherently contains diverse co-acting species. For example, Mg^{2+} ions and polycarboxylates are both known to influence calcium carbonate formation, and the study by Wolf et al. [67] showed that their combined presence leads to a marked synergistic effect. Specifically, polyaspartic acid in conjunction with Mg^{2+} strongly inhibits nucleation while simultaneously stabilizing amorphous mineral phases, an effect not observed when each additive is applied separately.

A long-standing question in the field of coral biomineralization is the extent to which environmental factors versus biological macromolecules govern the precipitation of the $CaCO_3$ mineral phase. As mentioned earlier, in seawater, the Mg/Ca molar ratio is approximately 5.2, and aragonite is generally considered the favored polymorph under these conditions, both thermodynamically and kinetically. Numerous studies conducted in simplified, inorganic systems have demonstrated that calcite tends to dominate at lower Mg/Ca ratios, whereas aragonite formation becomes increasingly likely as the ratio approaches or exceeds a value of four. These findings have led to the hypothesis that the dominance of aragonite in coral skeletons might be sufficiently explained by ambient seawater composition, without invoking biological control mechanisms. However, mounting evidence suggests that this view is overly simplistic. In vitro studies involving coral

acid-rich proteins (CARPs) have demonstrated that certain macromolecules isolated from coral skeletons can only induce aragonite formation in the presence of Mg^{2+}, indicating a combined interaction between the organic matrix and Mg^{2+} ions [69]. This behavior is distinct from that observed in mollusks, where organic macromolecules alone are sufficient for aragonite formation regardless of Mg^{2+} presence [49,50]. These findings point toward a biomineralization mechanism in corals that is fundamentally different from that of other aragonite-forming organisms. Thus, the question arises: is aragonite formation in corals primarily governed by the inorganic seawater-like environment (notably high Mg/Ca ratio), or do the SOMs from coral skeletons have an intrinsic capacity to direct polymorph selection, even in the absence of Mg^{2+}? Answering this question requires experimental systems that isolate and dissect the contribution of individual factors.

To address this, the main goal of this work was to investigate the influence of the water-soluble organic macromolecules (SOMs) extracted from the skeleton of symbiotic and asymbiotic corals on the process of spontaneous precipitation of $CaCO_3$ in the absence and presence of Mg^{2+} ions. Used SOMs were extracted from the skeleton of Mediterranean colonial coral species, symbiotic *Cladocora caespitosa* (SOM-CCA) and asymbiotic *Astroides calycularis* (SOM-ACL). Calcium carbonate precipitation system containing only constituent ions (calcium and carbonate) and co-ions (sodium and chloride) that mimics the simplest inorganic environment (in seawater and extrapallial solution of marine organisms) [70] was chosen as a model system. The choice of such a system enables the investigation of the effects of chosen SOMs on calcium carbonate precipitation and discerning of these effects from the contributions of other factors (e.g., nonconstituent ions present in seawater) in the formation of $CaCO_3$. Additionally, magnesium ions were also introduced into the system to investigate the combined effect of SOMs and Mg^{2+} on calcium carbonate precipitation. We hypothesized that due to the addition of the chosen SOMs into the $CaCO_3$ precipitation system, the polymorph composition and the morphology of spontaneously precipitated $CaCO_3$ will change. Also, we assumed that when SOMs and Mg^{2+} are both added into the precipitation system, they will have a combined effect on $CaCO_3$ precipitation, and that in the formation of aragonite, Mg^{2+} will have a dominant role. In order to achieve set goals, spontaneous precipitation of $CaCO_3$, which was followed by pH measurements, in the systems in which different concentrations of SOM-CCA and SOM-ACL or Mg^{2+} were added, was performed. The morphology of the obtained $CaCO_3$ precipitates has been analyzed by scanning electron microscopy (SEM), while the polymorphic composition and characterization of the solid phase have been determined using powder X-ray diffraction (XRD) and infrared spectroscopy (IR).

The obtained results will contribute to the understanding of the role of organic matrix and Mg^{2+} in the biomineralization process and show how simple changes in the composition of the $CaCO_3$ precipitation solution can influence and tune the extent of compositional as well as the morphological change in precipitated $CaCO_3$.

2. Experimental

2.1. Materials

In all the experiments, analytically pure chemicals $CaCl_2 \cdot 2H_2O$, $MgCl_2 \cdot 6H_2O \cdot NaHCO_3$, NaCl, and NaOH (purchased from Sigma–Aldrich, St. Louis, MO, USA), as well as deionized water (conductivity less than 0.055 $\mu S\ cm^{-1}$), were used. The soluble organic macromolecules from the skeletons of corals *Cladocora caespitosa* (SOM-CCA) and *Astroides calycularis* (SOM-ACL) were extracted as reported elsewhere [71]. Their biochemical composition, including SDS-PAGE electrophoretic profiles showing multiple protein fractions, has been described in detail by Reggi et al. [72].

2.2. $CaCO_3$ Precipitation Experiments

Calcium carbonate was precipitated by mixing equal volumes (200 cm^3) of $CaCl_2$ and $NaHCO_3$ solutions. The $CaCl_2$ solution was rapidly added to the $NaHCO_3$ solution. $CaCl_2$ solution was prepared by diluting the appropriate amount of 1.000 mol dm^{-3} $CaCl_2$ stock solution, while sodium bicarbonate solution was always prepared by dissolving the appropriate mass of anhydrous $NaHCO_3$ in water. The initial concentrations of the reactants, $CaCl_2$ and $NaHCO_3$, were $c_0(CaCl_2)$ = 0.010 mol dm^{-3} and $c_0(NaHCO_3)$ = 0.005 mol dm^{-3}. An appropriate amount of additives, SOM-CCA or SOM-ACL, was always added to the sodium bicarbonate solution. The concentrations of both macromolecules, (γ_0 (SOM-CCA or SOM-ACL)), added separately into the precipitation system, were 0.5 ppm, 1 ppm, 2 ppm, and 4 ppm.

In experiments with added Mg^{2+}, Mg^{2+} was added to the precipitation system at initial concentration of $c_0(MgCl_2)$ = 0.050 mol dm^{-3} so that the concentration ratio of magnesium and calcium ions corresponded to the ratio at which these ions are present in the seawater ($c_0(Mg^{2+})$:$c_0(Ca^{2+})$ = 5:1). Mg^{2+} was always added to the $CaCl_2$ solution. The concentrations of both macromolecules, added separately, into the system with Mg^{2+}, were 0.5 ppm.

The system without additives and Mg^{2+} was the model system. A model system containing only constituent ions (Ca^{2+} and CO_3^{2-}) and co-ions (Na^+ and Cl^-) was used to mimic a simplified inorganic environment similar to extrapallial fluid in marine organisms with respect to the concentrations of Ca^{2+} and CO_3^{2-} ions [70]. This approach allowed us to investigate the effects of SOMs on $CaCO_3$ precipitation under controlled conditions, minimizing interference from other ions typically present in extrapallial fluid or seawater.

To ensure identical initial conditions concerning supersaturation and pH, it was necessary to adjust both the initial ionic strength (I_c) and pH of the system. The initial ionic strength was set to I_c = 0.420 mol dm^{-3} in all the systems. This was achieved by the addition of a defined volume of a 3.000 mol dm^{-3} NaCl stock solution. In systems without Mg^{2+}, the initial NaCl concentration was $c_0(NaCl)$ = 0.435 mol dm^{-3}, whereas in magnesium-containing systems, $c_0(NaCl)$ was adjusted to 0.300 mol dm^{-3}. The total amount of NaCl was distributed equally between the two reactant solutions, i.e., half was added to the $CaCl_2$ solution and the other half to the $NaHCO_3$ solution. The initial pH in all the systems was adjusted to 8.90 by the addition of an appropriate volume of a 1.000 mol dm^{-3} NaOH stock solution.

The supersaturation, S, with respect to calcite, aragonite, and vaterite was S_C = 7.1 ± 0.4, S_A = 6.0 ± 0.3, and S_V = 3.7 ± 0.2. The supersaturation was expressed as $S = (\Pi/K_{sp}{}^0)^{1/2}$ with ion activity product, $\Pi = a(Ca^{2+}) \cdot a(CO_3^{2-})$, and thermodynamic equilibrium constant of dissolution of the particular $CaCO_3$ phase, $K_{sp}{}^0$. The activity coefficients of z-valent ions, y_z, were calculated by using a modification of the Debye–Hückel equation as proposed by Davies [73]. The detailed calculation procedure, which considers the respective protolytic equilibria and equilibrium constants, together with the charge and mass balance equations, has been described previously [3,10,12]. The molar concentrations and activities of relevant ionic species were calculated by using our algorithm for calculations of the solution composition (the results were compared with those obtained by VMINTEQ 3.0 when possible (available at https://vminteq.com/download/ (accessed on 30 July 2021)). Calculations were based on the known initial concentrations of $CaCl_2$, $MgCl_2$, $NaHCO_3$, NaOH, and NaCl, and initial pH. The following ionic species were considered: H^+, OH^-, CO_3^{2-}, HCO_3^-, $H_2CO_3{}^0$, $NaCO_3^-$, $CaCO_3{}^0$, $CaHCO_3^+$, $CaOH^+$, $CaCl^+$, Ca^{2+}, Mg^{2+}, $MgCO_3{}^0$, $MgHCO_3^+$, $MgCl^+$, $MgOH^+$, $Mg_2CO_3{}^{2+}$, Na^+, Cl^-, $NaHCO_3{}^0$, $NaCl^0$, and $NaOH^0$.

The experiments were performed at 21 °C (chosen as an average Mediterranean seawater temperature [74,75]) in a thermostated double-walled glass vessel (Šurlan laboratory

glass, Medulin, Croatia) with a 400 cm^3 capacity. The vessel was tightly closed with a Teflon cover, thus minimizing the exchange of carbon dioxide between the ambient air and the reaction system. Upon initiation of experiments (i.e., mixing equal volumes (200 cm^3) of $CaCl_2$ and $NaHCO_3$ solutions), the systems were continuously stirred at a constant rate using a Teflon-coated magnetic stirring bar (Biosan, Riga, Latvia). The progress of the reaction was followed by measuring the pH of the solution using a combined glass–calomel electrode (Red Rod, Radiometer Analytical, Lyon, France) connected to a digital pH meter (PHM 290, Radiometer, Radiometer Analytical, Lyon, France). The experiments were stopped after an approximately constant value of pH was achieved. The resulting suspension was filtered through a 0.22 µm cellulose nitrate membrane filter (Millipore Merck KGaA, Darmstadt, Germany), and the obtained precipitate was washed with small portions of water and dried at 105 °C. Induction time is defined as the period between mixing the reactants and the first observable change in the system, typically indicated by the appearance of turbidity due to the formation of a solid phase. This moment marks the onset of crystal growth and was further confirmed by a characteristic drop in pH associated with ion consumption during precipitation.

2.3. Characterization of $CaCO_3$ Precipitate

The mineralogical composition of the precipitates was analyzed by IR spectroscopy (Tensor II spectrometer, Bruker, Billerica, MA, USA) using KBr pellets (Sigma–Aldrich, St. Louis, MO, USA, and by X-ray diffraction of powdered samples (PXRD) The PXRD patterns were recorded by an Aeris Benchtop X-Ray Panalytical diffractometer (Malvern Panalytical Ltd., Malvern, United Kingdom) with Ni-filtered copper radiation, in Bragg–Brentano geometry. A drop of the sample was placed on a silicon zero-background holder, and patterns were recorded in the range 2θ = 5–70° with a step size of 0.05° and 10 s per step. For data treatment, the PANalytical High Score Plus software suite (Version 3.0) was used. The crystal morphology was observed by scanning electron microscopy (SEM) on a JEOL JSM-7000F instrument (Jeol Ltd., Tokyo, Japan). For the SEM observations, the dried samples were attached by sticky carbon tape to an aluminium stub.

3. Results and Discussion

In this study, the influence of two types of water-soluble macromolecules isolated from the skeletons of corals *Cladocora caespitosa* (SOM-CCA) and *Astroides calycularis* (SOM-ACL) on the spontaneous precipitation of $CaCO_3$ was investigated. Furthermore, a simplified model system mimicking extrapallial solution of marine organisms with respect to the concentrations of the Ca^{2+} and CO_3^{2-} ions ($c_0(Ca^{2+})$:$c_0(CO_3^{2-})$ = 10 mmol dm^{-3}:5 mmol dm^{-3}) [70] was used. It is known that Mg^{2+} ions are present in extrapallial solution as well as in seawater in a Mg/Ca molar ratio of 5:1, and at this ratio, aragonite, not calcite, is the kinetically favored precipitate [35]. To distinguish the effect of each factor contributing to the formation and properties of precipitated $CaCO_3$ and observe if SOMs that were isolated from corals' skeletons will select the aragonite polymorph formation without the presence of Mg^{2+} in the system, our model system did not contain Mg^{2+}. The influence of SOMs and Mg^{2+} on $CaCO_3$ precipitation has been estimated by identifying the changes in the kinetics of spontaneous precipitation of $CaCO_3$ and properties of the isolated solid phases.

3.1. Polymorphic Composition and Morphology of $CaCO_3$ in the Model System and System with Addition of Mg^{2+}

The composition and morphology of the precipitates isolated from the model system and the magnesium-containing system were analyzed by IR, XRD, and SEM. Figure 1 shows IR spectra (Figure 1a,b; blue line), X-ray diffractograms (Figure 1c,d; blue line)

and scanning electron micrographs with insets of higher magnification (Figure 1e,f) of the samples isolated from the model system (system without addition of SOMs and/or Mg^{2+}) (Figure 1a,c,e) and from the system with the addition of Mg^{2+} (Figure 1b,d,f).

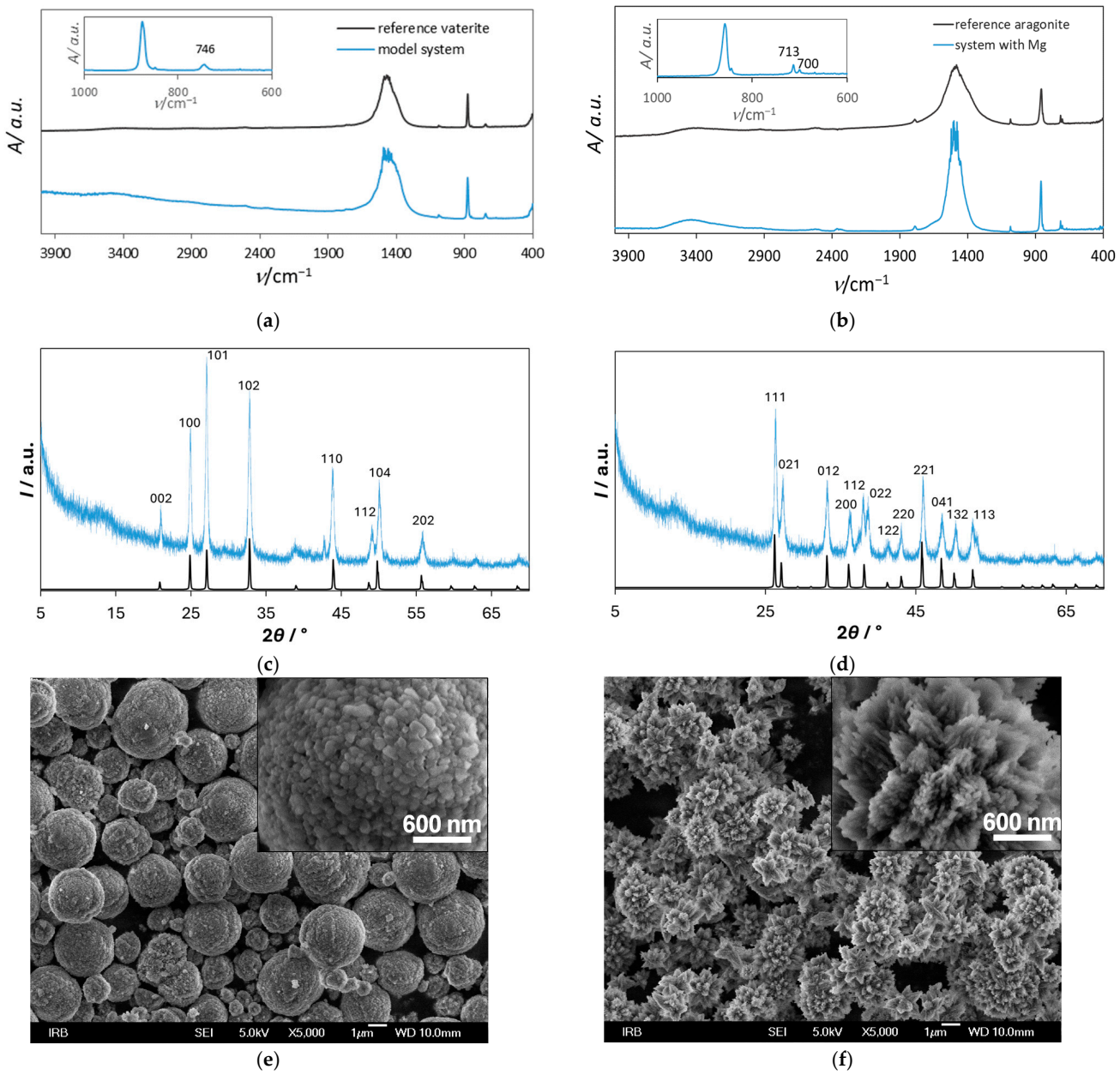

Figure 1. IR spectra (**a**,**b**; blue line), X-ray diffractograms (**c**,**d**; blue line), and scanning electron micrographs with insets of higher magnification (**e**,**f**) of spontaneously precipitated calcium carbonate in the model system (system without addition of SOMs and/or Mg^{2+}) with initial reactant concentrations $c_0(Ca^{2+})$ = 0.010 mol dm^{-3} and $c_0(CO_3^{2-})$ = 0.005 mol dm^{-3} (**a**,**c**,**e**) and in the system with the addition of Mg^2 with initial concentration of Mg^{2+}, $c_0(Mg^{2+})$ = 0.050 mol dm^{-3} (**b**,**d**,**f**). The reference IR spectra of pure vaterite and aragonite crystals (as reported in Refs. [12,36]) are shown as black lines in (**a**,**b**), respectively. The insets in (**a**,**b**) represent a specific wavenumber range of recorded IR spectra of obtained precipitates, and highlight the ν_4 carbonate bending region, showing characteristic absorption bands for vaterite at 746 cm^{-1} (**a**) and for aragonite at 700 and 713 cm^{-1} (**b**). X-ray reference patterns for vaterite and aragonite are shown as black lines in (**c**,**d**).

The results of the XRD analysis were in good agreement with FTIR analysis, and they indicated that in the model system, exclusively vaterite precipitated (Figure 1a,c), while in

the system with the addition of Mg^{2+}, only aragonite could be observed (Figure 1b,d). For comparison, the reference IR spectra of pure vaterite and aragonite crystals (as reported in Refs. [12,36]) are shown as black lines in (a) and (b), respectively. The insets in (a) and (b) display the characteristic ν_4 carbonate bending region of the recorded IR spectra of the obtained samples, with characteristic absorption bands at 746 cm^{-1} for vaterite (a), and at 700 and 713 cm^{-1} for aragonite (b), confirming the exclusive formation of these polymorphs in the respective systems. To enhance the clarity and comparability of the crystallographic data, X-ray reference patterns for vaterite and aragonite are also shown as black lines in (c) and (d). The XRD pattern of the sample on Figure 1c (blue line) shows the diffraction peaks at 2θ, 20.89°, 24.82°, 26.99°, 32.72°, 43.71°, 49.07°, 50.06°, and 55.74°corresponding to (002), (100), (101), (102), (110), (112), (104), and (202) diffraction lines of vaterite (JCPDS No. 33-0268). Similarly, the most prominent peaks on Figure 1d (blue line), were detected at 2θ, 26.2°, 27.2°, 33.2°, 36.1°, 37.9°, 38.4°, 41.4°, 42.8°, 45.8°, 48.7°, 50.2°, and 52.5° corresponding to (111), (021), (012), (200), (112), (022), (112), (220), (221), (041), (132), and (113) diffraction lines of aragonite (JCPDS card no. 411475).

SEM analysis showed that in the model system, typical spherical vaterite particles were formed (Figure 1e). As found earlier [4], spherical vaterite particles are compact aggregates of primary vaterite crystallites of 25–35 nm in size. Aragonite particles formed in a system with Mg^{2+} were also aggregates but of the irregular form (Figure 1f), just as observed in our previous paper [5]. They appeared organized radially. As indicated earlier [35], when performing crystallization experiments under ambient conditions, in systems with molar ratio of Mg/Ca equal to or greater than 4, (~5 is in the seawater) precipitation of aragonite is favored so the formation of pure aragonite in the system to which Mg^{2+} was added (and in such a large ratio to calcium) was the expected result. Since under these conditions the effect of Mg^{2+} is dominant, in the first part of our research, we primarily focused on the magnesium-free system, so that we could more precisely study the effect of the selected SOMs on calcium carbonate precipitation. Additionally, influence of SOMs was investigated in the $CaCO_3$ precipitation system with the addition of Mg^{2+}. The crucial advantage of applying such a strategy is not only the possibility to observe a noticeable effect of any ion or molecule individually, but also their possible combined effect on the calcium carbonate precipitation.

3.2. Effect of SOMs on Calcium Carbonate Precipitation

Addition of SOMs into the $CaCO_3$ precipitation system (without Mg^{2+}) caused changes in the course of precipitation. Because all the experimental parameters (such as initial pH, supersaturation, ionic strength, or temperature) were identical, the changes could be attributed exclusively to the influence of the additives.

The mineralogical composition of the calcium carbonate precipitates isolated from the magnesium-free precipitation systems into which SOM-ACL and SOM-CCA were added showed no significant difference from the respective model system, regardless of the SOM concentrations used and in the whole range of investigated concentrations of the selected SOMs, only vaterite precipitated, as was confirmed by the IR and X-ray analyses (Figure S1). It can be concluded that the addition of the selected SOMs did not induce any change in the phase composition of the precipitates within the investigated concentration range. Although both SOM-ACL and SOM-CCA were isolated from coral skeletons composed of aragonite, the obtained results suggest that the formation of aragonite was not promoted by the addition of the selected SOMs. This indicates that the selected SOMs alone may not be sufficient to induce aragonite formation, and thus are not solely responsible for its presence in coral skeletons. These findings are consistent with the observations reported

by Falini et al., who demonstrated that the coral acid-rich protein CARP3, when used in isolation, was unable to induce aragonite formation in the absence of Mg^{2+} [69].

The kinetics of spontaneous precipitation were followed by measuring the change in solution pH with time. Figure 2 shows the progress curves of precipitation processes recorded during the spontaneous precipitation of calcium carbonate in the presence of different SOM-ACL and SOM-CCA concentrations, in the systems without added Mg^{2+}. The dashed lines, corresponding to the calculated value of solubility of vaterite ((c_s (vaterite) = 8.744 mmol dm^{-3}) ≙ (pH = 7.835)) for the system without additives and under given conditions, are indicated. As can be seen, recorded pH progress curves have a similar shape. The first part of the curves, which is characterized by relatively constant pH, is related to the induction time after which a significant drop of pH could be observed, indicating that the crystal growth of $CaCO_3$ occurred. The final part of the curves is characterized, again, by relatively constant pH, indicating the termination of crystal growth of a specific crystal phase (in this case, vaterite). As can be seen from Figure 2, with the increase in concentration of added SOMs, the induction time increased, thus indicating the inhibition of the nucleation process. A detailed analysis of the recorded induction time as a function of each concentration of added SOMs, shown in Figure 3, reveals that in the systems to which SOM-CCA was added, the induction time, compared to the model system, increased significantly only at the highest concentration used, from 75 s (model system) to 140 s (4 ppm SOM-CCA). In contrast, a similar increase in induction time in the case of addition of SOM-ACL was already observed at 2 ppm SOM-ACL (t_{ind} = 135 s). At 4 ppm SOM-ACL induction time was 290 s, which is around a 3.9-fold increase compared to the model system. This indicates a stronger inhibitory effect of SOM-ACL on $CaCO_3$ precipitation. Although electrophoretic analysis was not performed as part of the current study due to limited sample availability, the SOM-CCA and SOM-ACL used here have been previously characterized using SDS-PAGE by Reggi et al. [72]. Their results revealed distinct protein profiles for each coral species, suggesting that the observed effects on $CaCO_3$ precipitation are indeed driven by specific organic components already identified in these extracts.

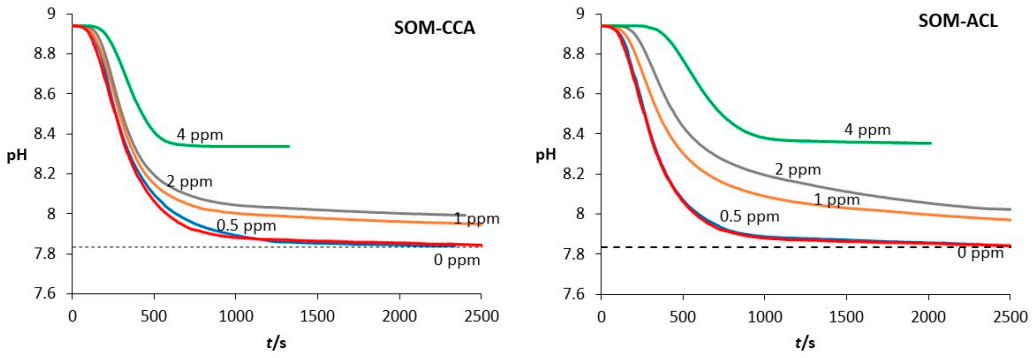

Figure 2. Progress curves, pH versus time, recorded during the spontaneous precipitation of $CaCO_3$ in presence of (**a**) SOM-CCA and (**b**) SOM-ACL, at 21 °C, in systems without added Mg^{2+} and with initial reactant concentrations $c_0(Ca^{2+})$ = 0.010 mol dm^{-3}, $c_0(CO_3^{2-})$ = 0.005 mol dm^{-3}. The concentrations of (**a**) SOM-CCA and (**b**) SOM-ACL added into the systems are expressed in ppm and written above the corresponding curves. The dashed lines correspond to calculated values of solubility of vaterite ((c_s (vaterite) = 8.744 mmol dm^{-3}) ≙ (pH = 7.835)) for the system without additives, under given conditions. The induction time corresponds to the initial plateau region of each pH curve, preceding the appearance of turbidity in the solution and the onset of a sharp pH drop.

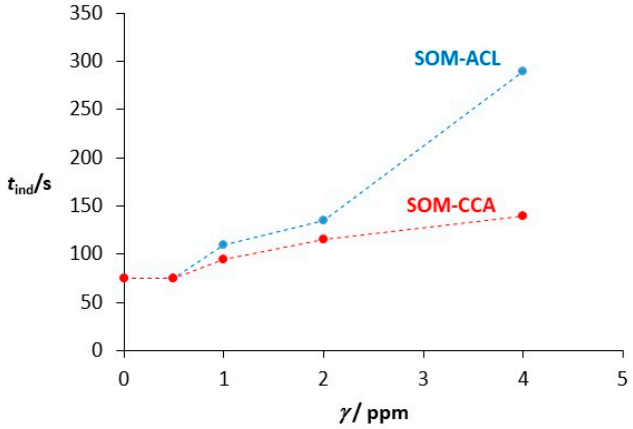

Figure 3. Induction time (t_{ind}) as a function of SOM concentration recorded in the $CaCO_3$ spontaneous precipitation systems, at 21 °C with initial reactant concentrations $c_0(Ca^{2+})$ = 0.010 mol dm^{-3}, $c_0(CO_3^{2-})$ = 0.005 mol dm^{-3} in the presence of different concentrations (γ/ppm) of SOM-CCA and SOM-ACL. Induction time was determined based on the appearance of turbidity in the solution and the onset of the pH drop in the titration curves (see Figure 2).

In case of both SOM-ACL and SOM-CCA, an increase in concentration caused the progressive lowering of the slope of the progress curves. Besides the lowering of the slope of the progress curves, the addition of both SOMs also led to the attainment of a relatively constant pH value in the final stage of the experiment, but at different final pH values. Moreover, as the concentration of SOMs increased, the final pH also increased. As can be seen from Figure 2, this pH was above the solubility of pure vaterite when concentrations of SOMs were γ_0(SOM-ACL or SOM-CCA) $\geq$ 1 ppm. A similar behavior of additives upon their addition to the $CaCO_3$ precipitation system was observed in studies investigating the effects of poly-L-aspartic acid [59] and a protein fragment isolated from the green organic layer of the mollusk shell *Haliotis rufescens* [5] on $CaCO_3$ precipitation. In the case of both additives, their observed influence on $CaCO_3$ precipitation was explained by the adsorption of the additives onto the growing $CaCO_3$ crystals.

3.3. Effect of SOMs on the Morphology of Precipitated Calcium Carbonate

To estimate the influence of added SOMs on spontaneously precipitated $CaCO_3$ in systems without Mg^{2+}, the morphology of the isolated $CaCO_3$ particles was also investigated by scanning electron microscopy. Figure 4 shows scanning electron micrographs of spontaneously precipitated calcium carbonate in the model system (without added Mg^{2+}) (Figure 4a) and with the addition of different concentrations of SOM-CCA (Figure 4b–d) and SOM-ACL (Figure 4e–g). In the model system, vaterite appears in the form of relatively regular spherulites with a rough surface (Figure 4a). Although the addition of both types of SOMs into the $CaCO_3$ precipitation system still resulted in vaterite spherulites, their morphology changed. Namely, SEM images show that the presence of SOMs induced the formation of vaterite spherulites with a more compact and smoother surface in comparison to the vaterite formed in the model system. The change in crystal morphology indicates strong interactions of SOMs with the crystal surface of the investigated crystals. In our previous investigations [29,59], smoothing of the surface of the vaterite particles, precipitated in the presence of polyamino acids (poly-L-aspartic acid (pAsp) and poly-L-glutamic acid (pGlu)), was also observed and could be related to the adsorption of pAsp and pGlu at the polycrystalline surfaces and subsequent formation of smaller primary particles. Also, when compared, different effects on morphology between the two SOMs could also be observed, just as in the case of induction time and inhibition of crystal growth. Namely, vaterite spherulites formed at the same SOM concentration (2 ppm) differ: vaterite spherulites in

the system with SOM-ACL have a smoother surface than the ones formed in the system with the same concentration of SOM-CCA. This corresponds to our observation of stronger inhibition of precipitation of vaterite with SOM-ACL than with SOM-CCA.

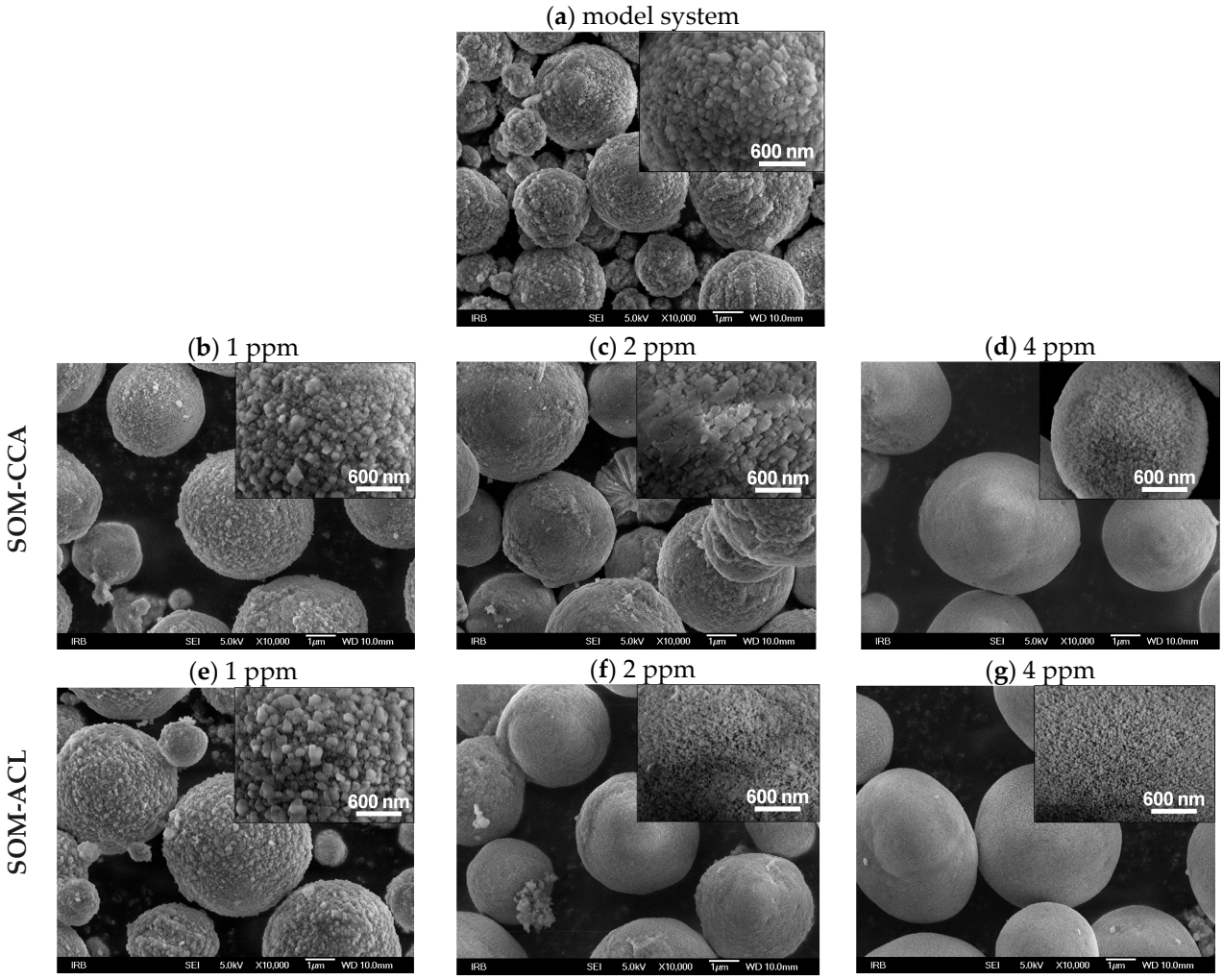

Figure 4. Scanning electron micrographs with insets of higher magnification of spontaneously precipitated calcium carbonate at 21 °C in the model system (**a**) with initial reactant concentrations $c_0(Ca^{2+})$ = 0.010 mol dm^{-3}, $c_0(CO_3{}^{2-})$ = 0.005 mol dm^{-3} and without added Mg^{2+} and in presence of different concentrations of SOM-CCA: 1 ppm (**b**), 2 ppm (**c**) and 4 ppm (**d**) and SOM-ACL: 1 ppm (**e**), 2 ppm (**f**) and 4 ppm (**g**).

3.4. Combined Effect of SOMs and Mg^{2+} on Calcium Carbonate Precipitation

Although the focus of the presented study has mainly been on the influence of the selected SOMs on $CaCO_3$ precipitation in a simplified system, crystals in living organisms typically grow under the influence of a combination of various additives. Recently, some bio-inspired studies have investigated the effects of combinations of these additives [65–67].

To investigate the combined effect of Mg^{2+} and the selected SOMs, the influence of the selected SOMs on $CaCO_3$ precipitation was investigated in the system with the addition of Mg^{2+}. In our previous investigation [76], a synergistic effect of Mg^{2+} and poly-L-aspartic acid (pAsp) on $CaCO_3$ precipitation at different initial pH was observed. Since pAsp was used as a model molecule for naturally occurring soluble acidic macromolecules of organic matrix involved in biomineralization processes, similar to the SOMs used in the present study, we assumed that when SOMs and Mg^{2+} are both added into the precipitation system, they will also have a combined effect on $CaCO_3$ precipitation. Figure 5 shows the $CaCO_3$

spontaneous precipitation progress curves in the system with added Mg^{2+}, as well as in systems with the addition of both Mg^{2+} and SOMs. Initial concentrations of reactants (Ca^{2+} and CO_3^{2-}) were as in the model system, and concentrations of added Mg^{2+} and SOMs were $c_0(Mg^{2+})$ = 0.050 mol dm^{-3} and (SOMs) = 0.5 ppm. A clear prolongation of the induction period is observed in the presence of additives: from 2500 s in the system with added Mg^{2+} to 13,000 s in the system with addition of Mg^{2+} and SOM-CCA, and 24,000 s in the system with addition of Mg^{2+} and SOM-ACL. Given that all the experimental parameters, namely, the initial pH, supersaturation, ionic strength, and temperature, were identical, the observed differences in induction time can be unequivocally attributed to the presence and interaction of the additives. A similar effect was found in the study by Wolf et al. [67], in which they showed that the combination of model macromolecule poly(aspartic acid) with Mg^{2+} led to synergistic effects and an increase in the efficiency towards inhibition of nucleation and growth of $CaCO_3$ precursors. The stronger hydration of magnesium ions compared to calcium ions may lead to an even stronger hydration of the precursors in combination with poly(aspartic acid) and inhibition of precipitation. These findings strongly suggest that Mg^{2+} may play a significant role in modulating the effectiveness of biological proteins in complex crystallization systems.

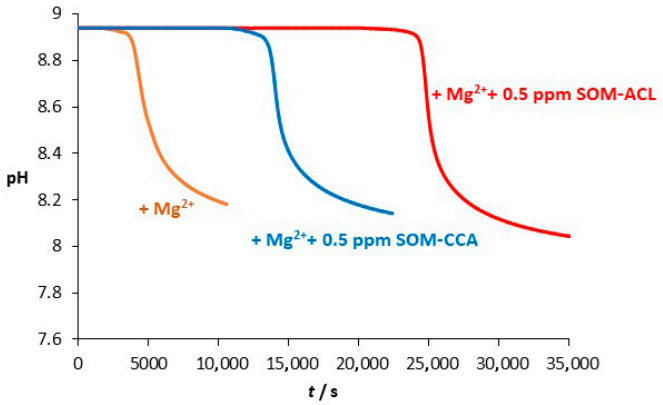

Figure 5. Progress curves, pH versus time, recorded during the spontaneous precipitation of $CaCO_3$ at 21 °C in a system with added Mg^{2+} (orange) and in a system with added Mg^{2+} and SOM-CCA (blue) or SOM-ACL (red). Initial concentrations of reactants $c_0(Ca^{2+})$ = 0.010 mol dm^{-3}, $c_0(CO_3^{2-})$ = 0.005 mol dm^{-3}, and $c_0(Mg^{2+})$ = 0.050 mol dm^{-3}. The concentration of added SOMs (SOM-CCA and SOM-ACL) was 0.5 ppm.

In the investigated concentration range of added SOMs, the mineralogical composition of the calcium carbonate precipitates isolated from the systems into which both Mg^{2+} and SOM-ACL or SOM-CCA were added showed no significant difference compared to precipitates isolated from the systems with the addition of only Mg^{2+}. In all the cases, only aragonite precipitated, as was confirmed by infrared spectroscopy and X-ray diffraction analysis (Figure S2). This can be explained by considering that, in our experiments, the Mg/Ca molar ratio was set to 5:1. It is well established that under ambient conditions, when the Mg/Ca molar ratio equals or exceeds 4 (similar to that found in seawater), aragonite is the kinetically favored $CaCO_3$ polymorph. In contrast, at lower Mg/Ca ratios, a mixture of calcite, magnesium calcite, and/or aragonite may form [35,36]. Therefore, the obtained results suggest that, within the investigated systems, the dominant effect on the mineralogical composition of the precipitate was exerted by Mg^{2+}.

Figure 6 shows scanning electron micrographs of spontaneously precipitated calcium carbonate in a magnesium-containing system without the addition of SOMs (Figure 6a,b), as well as with the addition of 0.5 ppm SOM-CCA (Figure 6c) and 0.5 ppm SOM-ACL (Figure 6d). Unlike the previously described system without Mg^{2+}, in which the addition

of SOMs caused a change in the morphology of the precipitated vaterite, in this system, the added macromolecules did not cause a visible change in the morphology of the precipitated aragonite. However, it should be noted that we were unable to conduct further investigations regarding the influence of these SOMs, at higher concentrations, on aragonite precipitation due to the very limited amount of SOMs available. Therefore, it would be incorrect to conclude that the selected SOMs do not affect the morphology of the precipitated aragonite. This is especially important considering that in our previous studies with similar SOMs, also isolated from corals, we observed that at higher concentrations (>5 ppm), they do alter the morphology of the precipitated aragonite [6].

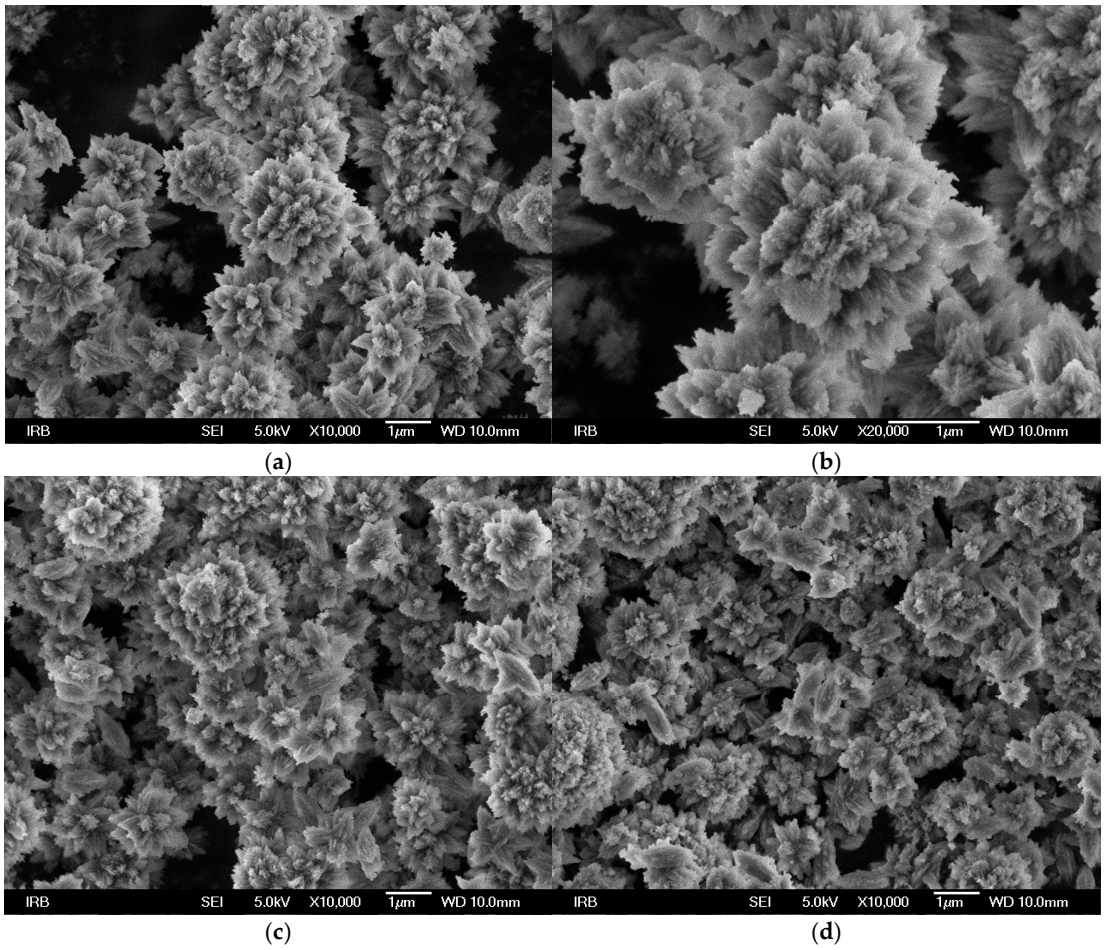

Figure 6. Scanning electron micrographs of spontaneously precipitated calcium carbonate in a system with Mg^{2+} with initial reactant concentrations $c_0(Ca^{2+})$ = 0.010 mol dm^{-3}, $c_0(CO_3{}^{2-})$ = 0.005 mol dm^{-3}, and $c_0(Mg^{2+})$ = 0.050 mol dm^{-3} without the addition of macromolecules (**a**,**b**) and with the addition of 0.5 ppm SOM-CCA (**c**) and 0.5 ppm SOM-ACL (**d**).

In order to further investigate the combined effect of SOMs and Mg^{2+} on $CaCO_3$ precipitation, a comparison of the recorded curves and induction times is shown in Figure 7 and Table 1. By comparing the kinetic curves recorded during spontaneous precipitation of $CaCO_3$ in the model system with the curves in systems with addition of only Mg^{2+} and only SOMs, as shown in Figure 7, it can be observed that under the given experimental conditions, a significant effect on the kinetics was observed in system with the addition of Mg^{2+} (t_{ind} increased from 75 s to 2500 s) in contrast to no effect on induction time when 0.5 ppm SOMs were added. Additionally, the increase in induction time, observed with the addition of Mg^{2+} into the system, became even more pronounced when both Mg^{2+} and SOM were added. These results indicate a combined inhibitory effect of SOMs and

Mg^{2+} on the kinetics of calcium carbonate precipitation. According to the literature, the observed combined effect is most likely caused by stronger hydration of magnesium ions compared to calcium ions, consequently leading to stronger hydration of the amorphous precursor phase, thereby inhibiting the formation of the crystalline phase [67]. It should also be noted that the strongest increase in induction time was observed in the system with the addition of SOM-ACL and Mg^{2+} (t_{ind} = 24,000 s), indicating, as observed earlier, stronger inhibitory effectiveness of SOM-ACL in comparison to SOM-CCA (t_{ind} = 13,000 s) on $CaCO_3$ precipitation. Since SOM-ACL and SOM-CCA are extracted from different coral species, observed results point to a species-specific interaction between SOMs and Mg^{2+}, which likely influences the characteristics of the mineral phase that forms the coral skeleton.

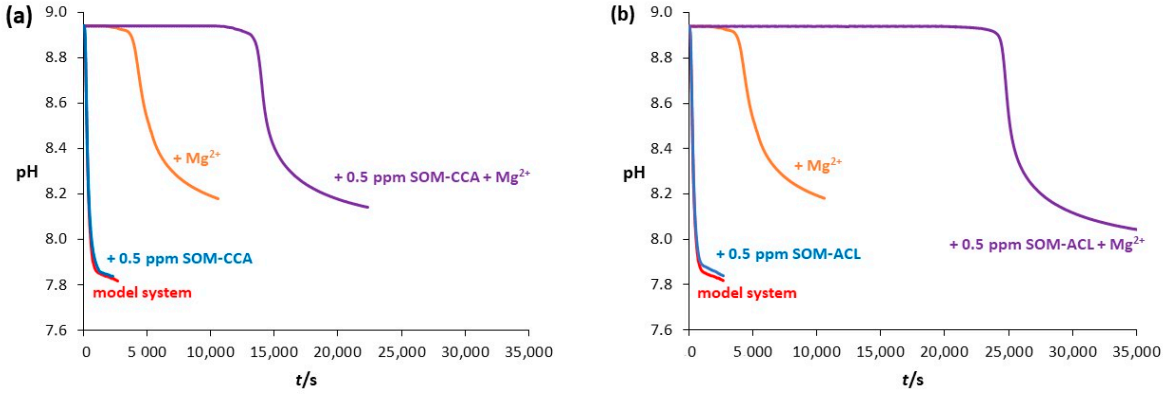

Figure 7. Progress curves, pH versus time, recorded during the spontaneous precipitation of $CaCO_3$ at 21 °C in: (**a**) the model system (without Mg^{2+} or SOMs (black line)), system with Mg^{2+} addition (orange line), system with SOM-CCA addition (blue line) and combined SOM-CCA + Mg^{2+} system (purple line); (**b**) the model system (without Mg^{2+} or SOMs (black line)), system with Mg^{2+} addition (orange line), system with SOM-ACL addition (blue line) and combined SOM-ACL + Mg^{2+} system (purple line). Initial reactant concentrations were $c_0(Ca^{2+})$ = 0.010 mol dm^{-3}, $c_0(CO_3^{2-})$ = 0.005 mol dm^{-3} and concentrations of added Mg^{2+} and SOMs were $c(Mg^{2+})$ = 0.050 mol dm^{-3} and γ(SOMs) = 0.5 ppm.

Table 1. Induction times (t_{ind}) observed during the spontaneous precipitation of $CaCO_3$ in system with initial reactant concentrations $c_0(Ca^{2+})$ = 0.010 mol dm^{-3}, $c_0(CO_3^{2-})$ = 0.005 mol dm^{-3} at 21 °C in the model system (without Mg^{2+} or SOMs) and in systems with addition of: SOMs or Mg^{2+} or combined (SOMs + Mg^{2+}). Concentrations of added Mg^{2+} and SOMs were $c_0(Mg^{2+})$ = 0.050 mol dm^{-3} and γ(SOMs) = 0.5 ppm.

ADDITIVE	t_{ind}/s
model system	75
0.5 ppm SOM-CCA	75
0.5 ppm SOM-ACL	75
Mg^{2+}	2500
0.5 ppm SOM-CCA + Mg^{2+}	13,000
0.5 ppm SOM-ACL + Mg^{2+}	24,000

4. Conclusions

This study explored the influence of water-soluble organic macromolecules (SOMs) extracted from the skeletons of two Mediterranean colonial coral species, symbiotic *Cladocora caespitosa* (SOM-CCA) and asymbiotic *Astroides calycularis* (SOM-ACL), on the spontaneous precipitation of $CaCO_3$, in systems both with and without Mg^{2+}. Using a simplified precipitation model system that mimics only the key ionic components of extrapallial fluid, namely calcium, carbonate, sodium, and chloride ions, allowed us to systematically investi-

gate the individual and combined effects of SOMs and Mg^{2+} on the precipitation kinetics, polymorphism, and morphology of $CaCO_3$ and to distinguish these effects from those that might arise from other ions typically present in extrapallial fluid.

In the model system, a system without Mg^{2+} or SOMs, only vaterite spherulites precipitated, and the addition of SOMs into the system did not significantly affect the polymorphic composition of the precipitates. However, it did result in inhibition of $CaCO_3$ precipitation and notable changes in the morphology of the precipitates. Indeed, between the two SOM types, SOM-ACL exhibited a stronger effect, manifested as a significant increase in induction time and a change in $CaCO_3$ morphology at the same SOM concentrations, suggesting a stronger interaction with the growing crystal surfaces compared to SOM-CCA.

When Mg^{2+} was introduced (Mg/Ca = 5:1), aragonite was the sole polymorph that precipitated, which is consistent with the known role of Mg^{2+} in stabilizing this phase under seawater-like conditions. The addition of SOMs to Mg-containing systems did not change the polymorphic composition of the precipitates but markedly enhanced the inhibition of precipitation, with the most pronounced increase in induction time observed in the system combining Mg^{2+} and SOM-ACL. This points to a combined effect of Mg^{2+} and SOMs on $CaCO_3$ precipitation, as the observed effects on induction time were more pronounced in systems where both components were present than in those where Mg^{2+} or SOMs were added individually. Moreover, since SOM-ACL exerted a stronger influence than SOM-CCA, both in the presence and absence of Mg^{2+}, it may be suggested that the interaction between SOMs and $CaCO_3$ is species-specific and likely contributes to defining the properties of the mineral phase that forms the coral skeleton.

Overall, the findings provide new insights into the physicochemical mechanisms underlying coral biomineralization and may support the development of biomimetic strategies for synthesizing functional mineralized materials.

Supplementary Materials: The following supporting information can be downloaded at https://www.mdpi.com/article/10.3390/colloids9040050/s1, Figure S1. IR spectra (a) and X-ray diffractograms (b) of spontaneously precipitated calcium carbonate in the system without Mg^{2+} and with addition of SOMs with initial reactant concentrations $c_0(Ca^{2+}) = 0.010$ mol dm^{-3}, $c_0(CO_3{}^{2-}) = 0.005$ mol dm^{-3}; Figure S2. IR spectra (a) and X-ray diffractograms (b) of spontaneously precipitated calcium carbonate in the system with initial reactant concentrations $c_0(Ca^{2+}) = 0.010$ mol dm^{-3} and $c_0(CO_3{}^{2-}) = 0.005$ mol dm^{-3}, and with addition of Mg^{2+}, Mg^{2+} + SOM-CCA, and Mg^{2+} + SOM-ACL.

Author Contributions: Conceptualization B.Nj.Dž., G.F. and S.G.; methodology B.Nj.Dž. and J.K.; validation B.Nj.Dž. and J.K.; formal analysis J.K., N.M.M., B.Nj.Dž. and A.S.; investigation B.Nj.Dž., J.K., N.M.M., A.S., D.K., S.G. and G.F.; resources, B.Nj.Dž., G.F. and S.G.; writing—original draft preparation, B.Nj.Dž. and J.K.; writing—review and editing, B.Nj.Dž., J.K., N.M.M., A.S., D.K. and G.F.; visualization N.M.M.; supervision B.Nj.Dž.; project administration B.Nj.Dž.; funding acquisition B.Nj.Dž., G.F. and S.G. All authors have read and agreed to the published version of the manuscript.

Funding: This research received no external funding.

Data Availability Statement: Data will be made available upon request.

Acknowledgments: This work has been supported by the Croatian Academy of Sciences and Arts Foundation grant and Unity through Knowledge Fund grant and has also, in part (G.F. and S.G.), been supported by the European Research Council Grant Agreement No. 249930–CoralWarm: Corals and global warming: the Mediterranean versus the Red Sea.

Conflicts of Interest: The authors declare no conflicts of interest.

References

1. Mann, S. *Biomineralization: Principles and Concepts in Bioinorganic Materials Chemistry*; Oxford University Press: New York, NY, USA, 2001; ISBN 0198508824.
2. Brečević, L.; Kralj, D. Kinetics and Mechanisms of Crystal Growth in Aqueous Systems. In *Interfacial Dynamics*; Kallay, N., Ed.; Surfactant Science Series; Marcel Dekker: New York, NY, USA, 2000; Volume 88, pp. 435–474; ISBN 0-8247-0006-6.
3. Njegić-Džakula, B.; Brečević, L.; Falini, G.; Kralj, D. Calcite Crystal Growth Kinetics in the Presence of Charged Synthetic Polypeptides. *Cryst. Growth Des.* **2009**, *9*, 2425–2434. [CrossRef]
4. Brečević, L.; Nöthig-Laslo, V.; Kralj, D.; Popović, S. Effect of divalent cations on the formation and structure of calcium carbonate polymorphs. *J. Chem. Soc. Faraday Trans.* **1996**, *92*, 1017–1022. [CrossRef]
5. Njegić-Džakula, B.; Reggi, M.; Falini, G.; Weber, I.; Brečević, L.; Kralj, D. The Influence of a Protein Fragment Extracted from Abalone Shell Green Layer on the Precipitation of Calcium Carbonate Polymorphs in Aqueous Media. *Croat. Chem. Acta* **2013**, *86*, 39–47. [CrossRef]
6. Njegić Džakula, B.; Fermani, S.; Dubinsky, Z.; Goffredo, S.; Falini, G.; Kralj, D. In Vitro Coral Biomineralization under Relevant Aragonite Supersaturation Conditions. *Chem.-A Eur. J.* **2019**, *25*, 10616–10624. [CrossRef]
7. Gower, L.; Tirrell, D. Calcium carbonate films and helices grown in solutions of poly (aspartate). *J. Cryst. Growth* **1998**, *191*, 153–160. [CrossRef]
8. Jie, P.; Zhiming, L. Influence of temperature on microbially induced calcium carbonate precipitation for soil treatment. *PLoS ONE* **2019**, *14*, e0218396.
9. Ruiz-Agudo, E.; Putnis, C.V.; Rodriguez-Navarro, C.; Putnis, A. Effect of pH on calcite growth at constant $a_{Ca}{}^{2+}/a_{CO3}{}^{2-}$ ratio and supersaturation. *Geochim. Cosmochim. Acta* **2011**, *75*, 284–296. [CrossRef]
10. Kontrec, J.; Tomašić, N.; Matijaković Mlinarić, N.; Kralj, D.; Njegić Džakula, B. Effect of pH and type of stirring on the spontaneous precipitation of $CaCO_3$ at identical initial supersaturation, ionic strength and $a(Ca^{2+})/a(CO_3{}^{2-})$ ratio. *Crystals* **2021**, *11*, 1075–1087. [CrossRef]
11. Zuddas, P.; Mucci, A. Kinetics of Calcite Precipitation from Seawater: II. The Influence of the Ionic Strength. *Geochim. Cosmochim. Acta* **1998**, *62*, 757–766. [CrossRef]
12. Kralj, D.; Brečević, L.; Nielsen, A.E. Vaterite growth and dissolution in aqueous solution I. Kinetics of crystal growth. *J. Cryst. Growth* **1990**, *104*, 793–800. [CrossRef]
13. Davis, K.J.; Dove, P.M.; De Yoreo, J.J. The Role of Mg^{2+} as an Impurity in Calcite Growth. *Science* **2000**, *290*, 1134–1137. [CrossRef]
14. Berner, R.A. The role of magnesium in the crystal growth of calcite and aragonite from sea water. *Geochim. Cosmochim. Acta* **1975**, *39*, 489–504. [CrossRef]
15. Morse, J.W.; Arvidson, R.S.; Lüttge, A. Calcium Carbonate Formation and Dissolution. *Chem. Rev.* **2007**, *107*, 342–381. [CrossRef] [PubMed]
16. Lowenstam, H.A. Minerals formed by organisms. *Science* **1981**, *211*, 1126–1131. [CrossRef] [PubMed]
17. Addadi, L.; Raz, S.; Weiner, S. Taking Advantage of Disorder: Amorphous Calcium Carbonate and Its Roles in Biomineralization. *Adv. Mater.* **2003**, *15*, 959–970. [CrossRef]
18. Cartwright, J.H.E.; Checa, A.G.; Gale, J.D.; Gebauer, D.; Sainz-Díaz, C.I. Calcium carbonate polyamorphism and its role in biomineralization: How many amorphous calcium carbonates are there? *Angew. Chem. Int. Ed.* **2012**, *51*, 11960–11970. [CrossRef]
19. Politi, Y.; Arad, T.; Klein, E.; Weiner, S.; Addadi, L. Sea urchin spine calcite forms via a transient amorphous calcium carbonate phase. *Science* **2004**, *306*, 1161–1164. [CrossRef]
20. Weiss, I.M.; Tuross, N.; Addadi, L.; Weiner, S. Mollusc larval shell formation: Amorphous calcium carbonate is a precursor phase for aragonite. *J. Exp. Zool.* **2002**, *293*, 478–491. [CrossRef]
21. Beniash, E.; Aizenberg, J.; Addadi, L.; Weiner, S. Amorphous calcium carbonate transforms into calcite during sea urchin larval spicule growth. *Proc. R. Soc. Lond. Ser. B Biol. Sci.* **1997**, *264*, 461–465. [CrossRef]
22. Dillaman, R.; Hequembourg, S.; Gay, M. Early pattern of calcification in the dorsal carapace of the blue crab, *Callinectes sapidus*. *J. Morphol.* **2005**, *263*, 356–374. [CrossRef]
23. Gebauer, D.; Volkel, A.; Colfen, H. Stable Prenucleation Calcium Carbonate Clusters. *Science* **2008**, *322*, 1819–1822. [CrossRef] [PubMed]
24. Kanakis, J.; Malkaj, P.; Petroheilos, J.; Dalas, E. Crystallization of calcium carbonate on porcine and human cardiac valves and the antimineralization effect of sodium alginate. *J. Cryst. Growth* **2001**, *223*, 557–564. [CrossRef]
25. Oliveira, A.M.; Farina, M.; Ludka, I.P.; Kachar, B. Vaterite, calcite, and aragonite in the otoliths of three species of piranha. *Naturwissenschaften* **1996**, *83*, 133–135. [CrossRef]
26. Ariani, A.P.; Wittmann, K.J.; Franco, E. A Comparative Study of Static Bodies in Mysid Crustaceans: Evolutionary Implications of Crystallographic Characteristics. *Biol. Bull.* **1993**, *185*, 393–404. [CrossRef]
27. Lambert, G.; Lambert, C.C. Spicule Formation in the New Zealand Ascidian *Pyura pachydermatina* (Chordata, Ascidiacea). *Connect. Tissue Res.* **1996**, *34*, 263–269. [CrossRef]

28. Qiao, L.; Feng, Q.L.; Liu, Y. A novel bio-vaterite in freshwater pearls with high thermal stability and low dissolubility. *Mater. Lett.* **2008**, *62*, 1793–1796. [CrossRef]
29. Njegić Džakula, B.; Falini, G.; Kralj, D. Crystal growth mechanism of vaterite in the systems containing charged synthetic Poly (Amino Acids). *Croat. Chem. Acta* **2017**, *90*, 689–698. [CrossRef]
30. Andreassen, J.-P. Formation mechanism and morphology in precipitation of vaterite—Nano-aggregation or crystal growth? *J. Cryst. Growth* **2005**, *274*, 256–264. [CrossRef]
31. Rodriguez-Blanco, J.D.; Shaw, S.; Benning, L.G. The kinetics and mechanisms of amorphous calcium carbonate (ACC) crystallization to calcite, via vaterite. *Nanoscale* **2011**, *3*, 265–271. [CrossRef] [PubMed]
32. Astilleros, J.M.; Fernández-Díaz, L.; Putnis, A. The role of magnesium in the growth of calcite: An AFM study. *Chem. Geol.* **2010**, *271*, 52–58. [CrossRef]
33. Balthasar, U.; Cusack, M. Aragonite-calcite seas—Quantifying the gray area. *Geology* **2015**, *43*, 99–102. [CrossRef]
34. Wang, D.; Hamm, L.M.; Giuffre, A.J.; Echigo, T.; Rimstidt, J.D.; De Yoreo, J.J.; Grotzinger, J.; Dove, P.M. Revisiting geochemical controls on patterns of carbonate deposition through the lens of multiple pathways to mineralization. *Faraday Discuss.* **2012**, *159*, 371–386. [CrossRef]
35. Kitano, Y.; Hood, D.W. Calcium Carbonate Crystal Forms Formed from Sea Water by Inorganic Processes. *J. Oceanogr. Soc. Japan* **1962**, *18*, 141–145. [CrossRef]
36. Fermani, S.; Njegić Džakula, B.; Reggi, M.; Falini, G.; Kralj, D. Effects of magnesium and temperature control on aragonite crystal aggregation and morphology. *CrystEngComm* **2017**, *19*, 2451–2455. [CrossRef]
37. Kimura, T.; Koga, N. Monohydrocalcite in comparison with hydrated amorphous calcium carbonate: Precipitation condition and thermal behavior. *Cryst. Growth Des.* **2011**, *11*, 3877–3884. [CrossRef]
38. Purgstaller, B.; Konrad, F.; Dietzel, M.; Immenhauser, A.; Mavromatis, V. Control of Mg^{2+}/Ca^{2+} Activity Ratio on the Formation of Crystalline Carbonate Minerals via an Amorphous Precursor. *Cryst. Growth Des.* **2017**, *17*, 1069–1078. [CrossRef]
39. Vereshchagin, O.S.; Frank-Kamenetskaya, O.V.; Kuz'mina, M.A.; Chernyshova, I.A.; Shilovskikh, V.V. Effect of magnesium on monohydrocalcite formation and unit-cell parameters. *Am. Mineral.* **2021**, *106*, 1294–1305. [CrossRef]
40. Bots, P.; Benning, L.G.; Rickaby, R.E.M.; Shaw, S. The role of SO4 in the switch from calcite to aragonite seas. *Geology* **2011**, *39*, 331–334. [CrossRef]
41. Wang, J.; Xu, Y.; Zhao, Y.; Huang, Y.; Wang, D.; Jiang, L.; Wu, J.; Xu, D. Morphology and crystalline characterization of abalone shell and mimetic mineralization. *J. Cryst. Growth* **2003**, *252*, 367–371. [CrossRef]
42. Politi, Y.; Batchelor, D.R.; Zaslansky, P.; Chmelka, B.F.; Weaver, J.C.; Sagi, I.; Weiner, S.; Addadi, L. Role of magnesium ion in the stabilization of biogenic amorphous calcium carbonate: A structure-function investigation. *Chem. Mater.* **2010**, *22*, 161–166. [CrossRef]
43. Mann, S. Molecular recognition in biomineralization. *Nature* **1988**, *332*, 119–124. [CrossRef]
44. Addadi, L.; Moradian, J.; Shay, E.; Maroudas, N.G.; Weiner, S. A chemical model for the cooperation of sulfates and carboxylates in calcite crystal nucleation: Relevance to biomineralization. *Proc. Natl. Acad. Sci. USA* **1987**, *84*, 2732–2736. [CrossRef]
45. Cölfen, H. Precipitation of carbonates: Recent progress in controlled production of complex shapes. *Curr. Opin. Colloid Interface Sci.* **2003**, *8*, 23–31. [CrossRef]
46. Addadi, L.; Joester, D.; Nudelman, F.; Weiner, S. Mollusk Shell Formation: A Source of New Concepts for Understanding Biomineralization Processes. *Chem.–A Eur. J.* **2006**, *12*, 980–987. [CrossRef]
47. Albeck, S.; Aizenberg, J.; Addadi, L.; Weiner, S. Interactions of Various Skeletal Intracrystalline Components with Calcite Crystals. *J. Am. Chem. Soc.* **1993**, *115*, 11691–11697. [CrossRef]
48. Gotliv, B.-A.; Kessler, N.; Sumerel, J.L.; Morse, D.E.; Tuross, N.; Addadi, L.; Weiner, S. Asprich: A novel aspartic acid-rich protein family from the prismatic shell matrix of the bivalve Atrina rigida. *ChemBioChem* **2005**, *6*, 304–314. [CrossRef] [PubMed]
49. Takeuchi, T.; Sarashina, I.; Iijima, M.; Endo, K. In vitro regulation of $CaCO_3$ crystal polymorphism by the highly acidic molluscan shell protein Aspein. *FEBS Lett.* **2008**, *582*, 591–596. [CrossRef]
50. Belcher, A.M.; Wu, X.H.; Christensen, R.J.; Hansma, P.K.; Stucky, G.D.; Morse, D.E. Control of crystal phase switching and orientation by soluble mollusc-shell proteins. *Nature* **1996**, *381*, 56–58. [CrossRef]
51. Feng, Q.L.; Pu, G.; Pei, Y.; Cui, F.Z.; Li, H.D.; Kim, T.N. Polymorph and morphology of calcium carbonate crystals induced by proteins extracted from mollusk shell. *J. Cryst. Growth* **2000**, *216*, 459–465. [CrossRef]
52. Politi, Y.; Mahamid, J.; Goldberg, H.; Weiner, S.; Addadi, L. Asprich mollusk shell protein: In vitro experiments aimed at elucidating function in $CaCO_3$ crystallization. *CrystEngComm* **2007**, *9*, 1171–1177. [CrossRef]
53. Song, R.-Q.; Cölfen, H. Additive controlled crystallization. *CrystEngComm* **2011**, *13*, 1249–1276. [CrossRef]
54. Jiang, W.; Pacella, M.S.; Athanasiadou, D.; Nelea, V.; Vali, H.; Hazen, R.M.; Gray, J.J.; McKee, M.D. Chiral acidic amino acids induce chiral hierarchical structure in calcium carbonate. *Nat. Commun.* **2017**, *8*, 15066. [CrossRef]

55. Green, D.C.; Ihli, J.; Kim, Y.-Y.; Chong, S.Y.; Lee, P.A.; Empson, C.J.; Meldrum, F.C. Rapid Screening of Calcium Carbonate Precipitation in the Presence of Amino Acids: Kinetics, Structure, and Composition. *Cryst. Growth Des.* **2016**, *16*, 5174–5183. [CrossRef]
56. Orme, C.A.; Noy, A.; Wierzbicki, A.; McBride, M.T.; Grantham, M.; Teng, H.H.; Dove, P.M.; DeYoreo, J.J. Formation of chiral morphologies through selective binding of amino acids to calcite surface steps. *Nature* **2001**, *411*, 775–779. [CrossRef] [PubMed]
57. Gower, L.B. Biomimetic Model Systems for Investigating the Amorphous Precursor Pathway and Its Role in Biomineralization. *Chem. Rev.* **2008**, *108*, 4551–4627. [CrossRef]
58. Kim, Y.-Y.; Freeman, C.L.; Gong, X.; Levenstein, M.A.; Wang, Y.; Kulak, A.; Anduix-Canto, C.; Lee, P.A.; Li, S.; Chen, L.; et al. The Effect of Additives on the Early Stages of Growth of Calcite Single Crystals. *Angew. Chem. Int. Ed.* **2017**, *56*, 11885–11890. [CrossRef] [PubMed]
59. Njegić-Džakula, B.; Falini, G.; Brečević, L.; Skoko, Ž.; Kralj, D. Effects of initial supersaturation on spontaneous precipitation of calcium carbonate in the presence of charged poly-l-amino acids. *J. Colloid Interface Sci.* **2010**, *343*, 553–563. [CrossRef] [PubMed]
60. Zou, Z.; Bertinetti, L.; Politi, Y.; Fratzl, P.; Habraken, W.J.E.M. Control of Polymorph Selection in Amorphous Calcium Carbonate Crystallization by Poly (Aspartic Acid): Two Different Mechanisms. *Small* **2017**, *13*, 1603100. [CrossRef]
61. Zou, Z.; Polishchuk, I.; Bertinetti, L.; Pokroy, B.; Politi, Y.; Fratzl, P.; Habraken, W.J.E.M. Additives influence the phase behavior of calcium carbonate solution by a cooperative ion-association process. *J. Mater. Chem. B* **2018**, *6*, 449–457. [CrossRef]
62. Yu, S.-H.; Cölfen, H. Bio-inspired crystal morphogenesis by hydrophilic polymers. *J. Mater. Chem.* **2004**, *14*, 2124–2147. [CrossRef]
63. Kim, Y.-Y.; Fielding, L.A.; Kulak, A.N.; Nahi, O.; Mercer, W.; Jones, E.R.; Armes, S.P.; Meldrum, F.C. Influence of the Structure of Block Copolymer Nanoparticles on the Growth of Calcium Carbonate. *Chem. Mater.* **2018**, *30*, 7091–7099. [CrossRef]
64. Cölfen, H.; Qi, L. A Systematic Examination of the Morphogenesis of Calcium Carbonate in the Presence of a Double-Hydrophilic Block Copolymer. *Chem.–A Eur. J.* **2001**, *7*, 106–116. [CrossRef]
65. Li, M.; Cölfen, H.; Mann, S. Morphological control of $BaSO_4$ microstructures by double hydrophilic block copolymer mixtures. *J. Mater. Chem.* **2004**, *14*, 2269–2276. [CrossRef]
66. Bawazer, L.A.; Ihli, J.; Comyn, T.P.; Critchley, K.; Empson, C.J.; Meldrum, F.C. Genetic Algorithm-Guided Discovery of Additive Combinations That Direct Quantum Dot Assembly. *Adv. Mater.* **2015**, *27*, 223–227. [CrossRef]
67. Wolf, S.L.P.; Jähme, K.; Gebauer, D. Synergy of Mg^{2+} and poly (aspartic acid) in additive-controlled calcium carbonate precipitation. *CrystEngComm* **2015**, *17*, 6857–6862. [CrossRef]
68. Marzec, B.; Green, D.C.; Holden, M.A.; Coté, A.S.; Ihli, J.; Khalid, S.; Kulak, A.; Walker, D.; Tang, C.; Duffy, D.M.; et al. Amino Acid Assisted Incorporation of Dye Molecules within Calcite Crystals. *Angew. Chem. Int. Ed.* **2018**, *57*, 8623–8628. [CrossRef] [PubMed]
69. Laipnik, R.; Bissi, V.; Sun, C.Y.; Falini, G.; Gilbert, P.U.P.A.; Mass, T. Coral acid rich protein selects vaterite polymorph in vitro. *J. Struct. Biol.* **2020**, *209*, 107431. [CrossRef] [PubMed]
70. Tracy, S.L.; François, C.J.P.; Jennings, H.M. The growth of calcite spherulites from solution I. Experimental design techniques. *J. Cryst. Growth* **1998**, *193*, 374–381. [CrossRef]
71. Goffredo, S.; Vergni, P.; Reggi, M.; Caroselli, E.; Sparla, F.; Levy, O.; Dubinsky, Z.; Falini, G. The Skeletal Organic Matrix from Mediterranean Coral Balanophyllia europaea Influences Calcium Carbonate Precipitation. *PLoS ONE* **2011**, *6*, e22338. [CrossRef]
72. Reggi, M.; Fermani, S.; Landi, V.; Sparla, F.; Caroselli, E.; Gizzi, F.; Dubinsky, Z.; Levy, O.; Cuif, J.-P.; Dauphin, Y.; et al. Biomineralization in Mediterranean Corals: The Role of the Intraskeletal Organic Matrix. *Cryst. Growth Des.* **2014**, *14*, 4310–4320. [CrossRef]
73. Davis, C.W. *Ion Association*; Butterworths: London, UK, 1962.
74. Sani, T.; Prada, F.; Radi, G.; Caroselli, E.; Falini, G.; Dubinsky, Z.; Goffredo, S. Ocean warming and acidification detrimentally affect coral tissue regeneration at a Mediterranean CO_2 vent. *Sci. Total Environ.* **2024**, *906*, 167789. [CrossRef] [PubMed]
75. García-Monteiro, S.; Sobrino, J.A.; Julien, Y.; Sòria, G.; Skokovic, D. Surface Temperature trends in the Mediterranean Sea from MODIS data during years 2003–2019. *Reg. Stud. Mar. Sci.* **2022**, *49*, 102086. [CrossRef]
76. Vojtkuf, I.; Andrašić, M.; Kralj, D.; Kontrec, J.; Njegić Džakula, B. Synergistic Effect of Additives in $CaCO_3$ Precipitation System at Different Initial pH. *Croat. Chem. Acta* **2024**, *97*, 175–187. [CrossRef]